Modelling and experimental investigation of high – pressure common rail diesel injection system

IOP Conf. Series: Materials Science and Engineering **973** (2020) 012037 doi:10.1088/1757-899X/973/1/012037

Modelling and experimental investigation of high – pressure common rail diesel injection system

W Niklawy[1], M Shahin[2], MI Amin[3] and AElmaihy[3]
[1] PhD candidate, Mechanical Power Engineering Department, Military Technical College, Cairo, Egypt.
[2] Mechanical Engineering Department, School of Engineering, Badr University, Badr, Cairo, Egypt.
[3] Mechanical Power Engineering Department, Military Technical College, Cairo, Egypt
niklawywaleed@gmail.com

Abstract. The high-pressure Common Rail (HPCR) injection system was originally introduced for diesel engines to both reduce pollutant emissions and enhancement of performance. HPCR separates fuel pressurization and injection processes from each other. The high injection pressure generated by the common rail system provides better atomisation and evaporation of fuel spray, resulting in improved air inlet and fuel jet mixing, which is advantageous for lowering soot emission. In this paper, a mathematical common rail injection system model has been presented. A Simulink/Matlab code was developed to execute this simulation. This work does not only seek to validate the presented numerical model but to have more insight for understanding the overall common rail injection system diesel engine performance under different operating conditions. Some simulation results are illustrated to highlight modelling capability.The engine used is an HCCI turbocharged diesel engine, 2776 cc, 4-stroke, and 4-cylinder, water-cooled with overhead valve mechanism. The common rail pressure, fuel consumption, start and duration of each injection through one engine cycle are measured at various engine speed and loads. The measured common rail fuel pressure and consumption are used to validate the simulation results. The findings of the simulation show good consistency with the experimental results. At last, some simulation results, which highlight the modelling capability, are illustrated at certain values of engine speed and load.

1. Introduction

Nowadays the HPCRS is the state-of-the-art technology used in most of the recently manufactured diesel engines. It came out as a way out for simultaneous improving diesel engine emissions with which the manufactures could reach the emission standards and allowing noise and performance to be improved. It provides more flexibility than any other used injection system [1-3]. In HPRCS, The pressure inside the common-rail is considered as the main fuel-injection measurement parameter. It also determines the injection -fuel pressure. The stabilization and excessive reaction of the common-rail pressure would affect all the engine regimes such as starting. Idling and acceleration[4]. Considering the preceding circumstances, the performance prediction of common rail equipment is of real significance in the design of the automotive engine to better understand the performance of diesel engine equipped with common rail, and the mechanisms that potentially can contribute to improved fuel consumption and reduced emissions through numerical simulations and experimental

work. Numerical simulations of the fuel injection process become more and more essential as computational power especially with the enormous development of computation recourses contrary to prohibitively expensive and time-consuming experiments. The numerical simulation results after validation can be extended and used alone to predict some of the engine performance parameters.

Currently there are many computational and numerical methods for modeling and simulating the injectionsystem[5]. Different models can be developed by identification based on experimental data, whether linear or nonlinear. Automotive applications of such models do not consider modeling the injection system alone but mainly the whole engine modeling. Nicolao et al [6] designed a nonlinear idle speed regulator by using an integrated approach to identify a NARX (Nonlinear Auto Regressive Exogenous) model of an internal combustion engine. Maione et al [7], concluded that the nonlinear identification approach is a promising modeling technique for the injection system too.

Computational Fluid Dynamics (CFD) has evolved as a consistent and cost-effective tool that is now regularly utilized in the perfection of new or enhanced engine designs. While CFD methods are a practical way to explore the performance of an engine at a particular operating condition, they may need high computational recourses when used as an engine optimization tool, where numerous operating points may have to be evaluated. Therefore, engine optimization demands a special computationally efficient algorithm [8]. To investigate the effect of the injection system on the combustion process, it is frequent to combine the CFD analyses with the experimental study [9]. This approach can get validated results of different phenomena within the cylinder such as temperature distribution, fuel evaporation process, flame zones, and spray cloud profile and emission concentrations [10] .With such investigation of combustion and spray processes, it could be promising to achieve the desired emission formation reduction [11] and to have more insight on the effect different fuel injection strategies on the combustion process [12]

Chiavola and Giulianelli [13] , Mulemane et al [14] and Lino et al [15] used the Advanced Modeling Environment for Simulation environment (AMESIM) [16] to simulate the common rail injection system, which is a design package that permits the exploration of systems by using different models of distinct elements ready-made or self-made component libraries. Each injection system component has a mathematical model, including different effects of frictions and leakages. The aim of these models is to investigate system dynamics, to conduct parametric analysis and system components geometric optimization, to predict and confirm the impact of operational circumstances on the injection process. Even so, even with good evaluation capabilities, they could not be considered as proper approaches for control as they do not provide any mathematical representation of the process dynamics.

Phenomenological models, such as lumped parameters or one-dimensional model [4,17-19] are based on simple schemes. They take the full benefit of the experimental measurements that, usually, are represented by comprehensive quantities and are capable to catch the fundamental aspects of the phenomenology [9]. So, they may be considered as the optimum models which compromise between the validity of model results and the required computational recourses since.

Lino et al [20] proposed a model for diesel engine Common Rail injection system, appropriate for control purposes. It is based on a lumped parameter representation. It has the capability to be modified to other injection systems with the alike structural design, only by identification of satisfactory geometrical parameters. They concluded that their model accuracy is adequate to estimate the system performance to check the controller performances. The obtained results were validated with those obtained through the AMESIM.Due to the lack of experimental data, they considered that the AMESIM model presented in[21] is a reliable demonstration of the real injection system as it accurately predicts the system dynamics.

Wang et al [4] developed a mathematical modeling approach and common-rail regulation of common-rail HPCRIS. The proposed system that comprises three components of the Sub-system high pressure pump, common rail subsystem, and injector subsystem was done in Matlab/Simu- link. The model validation was conducted by comparing the model results with those obtained by

AMESim.As noted from literature most of the models presented were validated either with AMESim [4,13,15,20] or with injection rate test bench [14,18,19].

In this paper a mathematical lumped parameter model is built for a common rail injection system. The proposed HPCRS includes four sub-systems namely; high pressure pump, common rail, injector, and injections timing. To The model is implemented in Matlab/Simulink.

The experimental work does not only used for validating the presented numerical model but also to have more insight for understanding the overall engine performance using a common rail injection system under different loads and speeds. The experimental work was conducted on a complete rig for testing common rail turbocharged HCCI diesel engines. The test rig includes the engine and all the instrumentation necessary for measuring and recording a macro as well as micro-operating parameters.

The novelty of this work is the use of measured in-cylinder pressure obtained from the test rig instead of using constant values as in [4,20]. The multiple injection strategy are employed in this work .The injections start times and durations are expressed in the model as a functions of load and engine speed by data regression obtained from experimental measurements. Finally, the numerical results are validated with experimental results obtained from a complete diesel engine test rig instead of using AMESim injection rate test bench results.

The paper organization as follows. A brief description of the test rig experimental set up in the next section. a detailed description of the model is illustrated in section 3. Section 4 sets outthe validation of the model and to prove the performance of the model. The capability of the model is introduced in section 4. In section 5, the conclusion and future work is outlined

2. The Test Facility (Experimental Setup)

Experimental investigations were conducted on a transport diesel engine of type VM Motri with an open chamber. Four in-line cylinders water-cooled direct injection diesel engine with over-head valve gear and “common rail” fuel injection system. (Available in the laboratory of mechanical power and energy at the Military technical college) The main engine design parameters are listed in Table 1. The test rig includes the engine and all the instrumentation necessary for measuring and recording the operating parameters. An on-line data acquisition system is furnished to improve the speed and accuracy of data collection and recording. is used. Table 1displays engine specifications.

Table 1.Engine specifications.

Description	**Specification**
Engine	R2816K5A
Bore	94 mm
Stroke	100 mm
weight	270 kg
Compression Ratio	17.5
Number of Cylinders	4
Displacement	2776 cc
Max power	90 kW (120H.P.) @ 3800 RPM
Peak Torque	400 N·m @ 1800 RPM
Fuel primary pump	Electric pump
Fuel System	Direct Fuel Injection Common Rail System
High-Pressure Fuel Pump Injection Timing System	Radial Piston Pump (3 pistons) CP3 2nd Generation Valve Belt Driven DOHC Overhead Camshafts

2.1 Instrumentations

The parameters measured are classified into three main groups. a -External parameters: Engine speed, engine load, fuel consumption, airflow, crank angle, ambient conditions and real-time. B-Internal parameters: pressure inside the cylinder, inlet and exhaust manifolds and fuel

line,andturbocharger speed. C-Safety parameters: Lubricating oil pressure and temperature, and cooling water, temperature. Figure 1 gives a general scheme showing numbered locations where important pickups and transducers are positioned. A list of these locations and the corresponding measured parameter used in this study at each is given below is given in table 2.

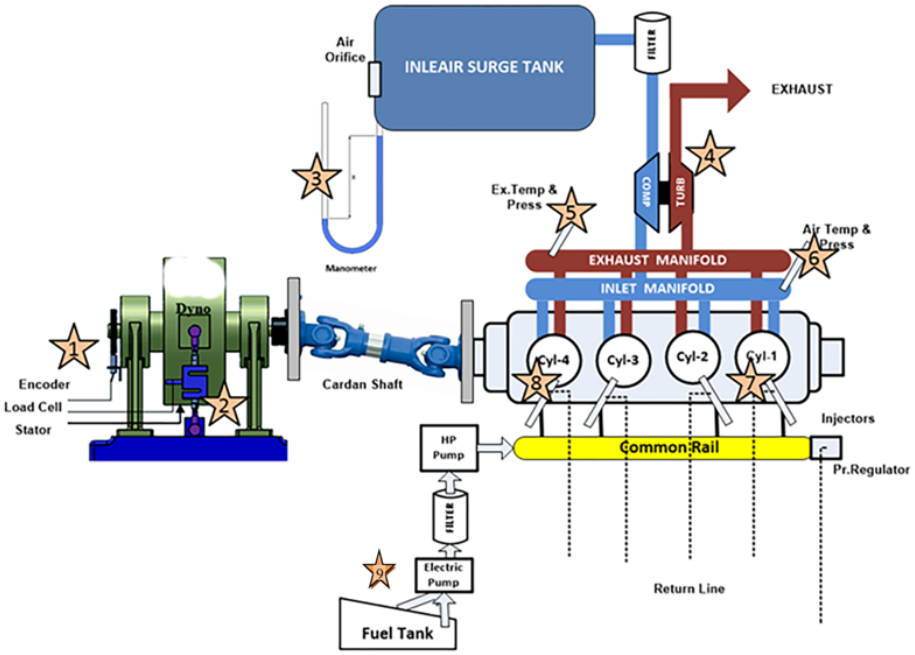

Figure 1. Test Facility Scheme

Table 2. A list of measured parameters and the corresponding locations relevant to figure 1

Location	Measured Parameters	Instrument	Accuracy
1	Engine Speed & Crank Angle	Incremental Encoder (WD GI 58B)	+ 7.5 % of the pulse width
2	External load (Torque)	S-type load cell	Combined error $\leq$+0.05%
7	Cylinder pressure	piezoelectric transducer type PCB (model no. 112B11)	<2.0 % FS
8	Fuel pressure sensor	piezoelectric transducer type (Kistler PN 6278)	<0.2 % FS
9	Fuel Consumption	Calibrated Bowel	NA

Engine external loading was carried out by an ELZE /Heenan hydraulic dynamometer. The fluid used was water with which the maximum braking power could reach 170 kW at 4000 rpm. The engine and dynamometer shafts were directly coupled through a cardan shaft. An S-type load cell (strain gauge type, max capacity 500kg) is inserted under the dynamometer torque reaction arm. The load cell is completed with a bridge amplifier that is excited (12VDC) from a regulated power supply. The whole setup is calibrated by applying known weights on the cell and observing the net voltage output.

A water-cooled piezoelectric transducer (type PCB model no. 112B11) is used for measuring cylinder pressure. The charge amplifier used is a PCB type, with the capability of statically holding the output charge for calibration processes.

A piezoelectric transducer type (Kistler PN 6278) and charge amplifier type (Kistler SN 284625) is used to measure fuel line pressure. This setup is capable of measuring pressure up to 3000 bars. The transducer is directly mounted on the high-pressure fuel line connecting the common rail to injector no.1. The transducer, amplifier, and cabling were calibrated together using a deadweight tester

Engine fuel consumption at steady-state operation is evaluated by recording the time of consumption of a certain volume of fuel. This old method remains particularly valuable today because of the high accuracy achieved. The measuring device consists of a glass flask of 250 cc volumes, an auxiliary fuel tank, a control cock, and a stopwatch.

An incremental digital quadrature encoder (type WDG 58B-360-ABN-G24-K3) is used for engine speed measurement. The encoder gives 2 trains of pulses (A and B), each has 360 pulses per encoder shaft revolution. The two trains are phased by ¼ pulses, and a third index train (N) with one pulse per each revolution is also produced. The Encoder is mounted on a special bracket fixed at the free end of the dynamometer shaft, figure 1.

2.2 Test procedure

Measured parameters included in this paper are engine speed, engine power (calculated from the dynamometer reading), fuel consumption, fuel line pressure, and cylinder pressure. The measurements were carried out at a fixed speed and engine load. The test procedure is required to fulfill the following main tasks in the prescribed order: first, pre-operational checks and preparations. Then, running the engine and sustaining the operating conditions as requested,(speed and load). Finally. Safety monitoring, e.g. overheating over-speed and overload.

3. Modeling

HPCR aims to deliver fuel with adequate high-pressure according to the engine operating condition. The system structure is indicated in figure 2. It consists of a high-pressure pump, a common rail, and injectors with their electronic control units. The fuel flow pressure is supplied from the tank to the pump with high pressure, where the fuel pressure goes up to the optimal high pressure. The high-pressure pump supply fuel with high-pressure to the rail, which distributes the fuel to each injector which in turn injects fuel with high-pressure to the cylinder. ECU determines the pressure of fuel based on the operational condition of the engine according to various engine sensor signals. HPCRS has a multifaceted injection process. The performance of the fuel injection system is affected by many factors, such as various components fuel leakage, fuel pipe elastic deformation due to high pressure, high temperature fuel compressibility and loss of high pressure and flow rate when the fuel flows through a variable cross-section etc.

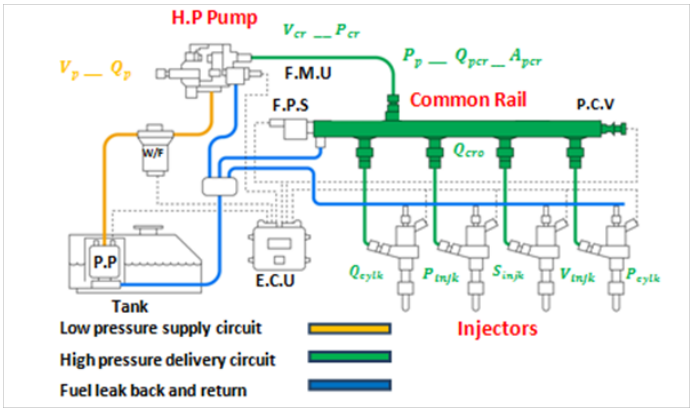

Figure 2.Common Rail Layout.

Some simplified assumptions are given base in system characteristics: the temperature variation of fuel is ignored throughout operations to ensure that system condition can be defined by its pressure; neglecting any pipe flow fluid dynamic phenomena, constant pressure of low-pressure pump is set [4, 20] but the in-cylinder pressure was taken from the experimental measurement in correspondence with engine load and speed. The HPCR model which contains four sub-models is constructed on the basis of the continuity equation, momentum equation and Newton's motion law.
The compressibility of the fuel demonstrated by the elasticity bulk modulusE is

$$E = -\frac{dP}{dV/V} = \frac{dP}{d\rho/\rho} \quad (1)$$

E is calculated as s function of fuel pressure P [22,23], in this work E is taken as 32500 bars from
From (1), the fuel pressure time derivative can be expressed as

$$\frac{dP}{dt} = -\frac{E}{V}.\frac{dV}{dt} \quad (2)$$

Where:
VIs the compartment instantaneous volume $\frac{dV}{dt}$ express the time rate of volume variation caused by moving boundaries and the difference between inlet and the outlet flows.
So equation (2) can be rewritten as

$$\frac{dP}{dt} = -\frac{E}{V}\left(\frac{dV_i}{dt} - Q_{inlet} + Q_{outlet}\right) \quad (3)$$

Q : The volumetric flow rate
$inlet\ and\ outlet$: are for intake and outtake flows respectively
$\frac{dV_i}{dt}$: The time rate of instantaneous volume due to moving boundaries,
$\frac{dP}{dt}$: The time rate of high-pressure pump, common rail pipe and injector.
Equation (3) is the fundamental equation of pressure dynamics in every control volume.
Excluding the high-pressure pump, all boundaries in HPCRIS are fixed (i.e.$\frac{\mathrm{dV_i}}{\mathrm{dt}} = 0$).
Using the basic conservation lawQ_{inlet} and Q_{outlet} can be written as

$$Q = sign(\Delta P).c_d.A.\left(\frac{2|\Delta P|}{\rho}\right)^{1/2} \quad (4)$$

Where sign (ΔP) is a sign function which accounts for the direction of flow,
C_d Coefficient of discharge
A Orifice sectional area
ρ Fuel density
ΔP Fuel pressure differential over the orifice.

3.1 High-pressure pump (HPP)
It is composed of three plunger pump connected on one shaft with 120° phase angle. The pump speed depends on the engine speed as the pump is driven by the camshaft. It is linked to the low and high-pressure circuits by a small orifice and a delivery check valve with a conical seat respectively.
From equation (3) the fuel pressure time derivative is

$$\frac{dP_p}{dt} = -\frac{E}{V_{pi}}\left(\frac{dV_{pi}}{dt} - Q_p + Q_{pcr} + Q_{pl}\right) \quad (5)$$

Where, the subscripts denote the following
p for HPP
i for instantaneous
pcr for HPP outlet fuel flow to the common rail
pl for fuel leakage flow
The instantaneous volume of the HPP V_{pi} is expressed according to the camshaft motion by

$$\frac{dV_{pi}}{dt} = -A_p\omega\frac{dh_p}{d\Theta} \quad (6)$$

A_p Sectional area of HPP plunger, $A_p = \frac{\pi}{4} d_p^2$

d_p Diameter of HPP plunger,

h_p HPP plunger displacement obtained from the kinematics of the plunger as a nonlinear function of the angular position and speed of the camshaft.

ω Angular camshaft speed,

θ Camshaft angular position

From Eq. (4) the HPP Fuel outlet flow to the Common Rail Q_{pcr} is given by

$$Q_{pcr} = sign(P_p - P_{cr}) c_{dcr} A_{pcr} \left(\frac{2}{\rho}|P_p - P_{cr}|\right)^{1/2} \quad (7)$$

Where, the subscripts CR denote common rail and p for pump

c_{dcr} Discharge coefficient which hanges with the pressure ratio in steady operational condition of the diesel engine. In this paper, it is set as a constant [4, 20].

A_{pcr} Area of the delivery valve connecting the pump and the high-pressure circuit,

$$\text{Sign } (P_p\text{-}P_{cr}) = \begin{cases} 0 & if P_p \le P_{cr} \\ 1 & if P_p > P_{cr} \end{cases} \quad (8)$$

The sign function determines the flow direction, when$P_p \le P_{cr}$, the delivery check valve (directional valve) between the HPP and CR closes to prevent the fuel flow from the rail to the HPP.

The HPP leakage flow Q_{pl} can be constant [4, 20][4,20].

So combining (5)–(8), Eq. (5) can be rephrased as

$$\frac{dP_p}{dt} = \frac{E}{V_{pi}} \left(A_{pcr} \omega \frac{dh_p}{d\theta} + Q_p - sign(P_p - P_{cr}) c_{dcr} A_{pcr} \left(\frac{2}{\rho}|P_p - P_{cr}|\right)^{1/2} - Q_{pl} \right) \quad (9)$$

3.2 Common rail subsystem

The rail pressure equilibrium is obtained by considering the relation between the inlet flow of the high-pressure pump and the outlet flows of the injector. Based on (3), the fuel pressure time derivative of common-rail can be modeled as

$$\frac{dP_{pcr}}{dt} = \frac{E}{V_{cr}} \left(Q_{pcr} - Q_{cro} - Q_{crb} \right) \quad (10)$$

Where, the subscripts denote the following

cr Common rail pipe

cro Common rail pipe outlet flow rate that is equal to the injectors he inlet fuel flow rate

crb Return flow, which is considered to be constant[4]

$$Q_{cro} = \sum_1^4 Q_{crok} \quad (11)$$

k injector number , k=1,2,3 and 4.

Q_{crok} Injection flow of each injector

$$Q_{crok} = sign(P_{pcr} - P_{injk}) c_{dinjk} A_{crik} \left(\frac{2}{\rho}|P_{cr} - P_{injk}|\right)^{1/2} \quad (12)$$

Where the subscript $injk$ is for the k[th] injector

c_{dinjk} Discharge coefficient of the orifice between common rail and k[th] injector,

A_{crik}Inlet port cross-sectional region in the k[th] injector.

Hence, Eq. (10) can be rewritable as

$$\frac{dP_{cr}}{dt} = \frac{E}{V_{cr}} \left(Q_{pcr} - \sum_1^4 sign(P_{cr} - P_{injk}) C_{dinjk} A_{crik} \left(\frac{2}{\rho}|P_{cr} - P_{injk}|\right)^{1/2} \right) \quad (13)$$

3.3 Injector subsystem

The common rail deliveries four injectors, one for each cylinder of the engine. Following from (3), the fuel pressure dynamics of the injector is shown as

$$\frac{dP_{injk}}{dt} = \frac{E}{V_{injk}}\left(Q_{crok} - Q_{cylk}\right) \quad (14)$$

Q_{cylk} fuel injection flow from the k[th] injector to a cylinder shown as

$$Q_{cylk} = sign\left(P_{injk} - P_{cylk}\right)E_{tk}c_{dik}A_{injk}\left(\frac{2}{\rho}|P_{injk} - P_{cylk}|\right)^{1/2} \quad (15)$$

Where the subscript $_{cylk}$ is for the k[th] cylinder

c_{dik} Discharge coefficient of the injector nozzle

A_{injk} Orifice area of the nozzle of the injector.

E_{tk} Square signal that equals to1 during injections and zeroes otherwise. It represents the time interval at which the injection outlet orifice is open. The injection duration $\theta_{injection,\ i}$ or $dt_{injection,\ i}$ in this work is related to the engine speed and load. Where $\theta_{injection,\ i}$ is the crank angle duration in degrees on which the injector orifice is open and $dt_{injection,\ i}$ is the time duration in [ms] on which the injector orifice is open.

Substitutes equations (12) and (15) in equation (14) ,results in

$$\frac{dP_{injk}}{dt} = \frac{E}{V_{injk}}\left(Q_{crok} - sign\left(P_{injk} - P_{cylk}\right)E_{tk}\mu_{ik}S_{injk}\left(\frac{2}{\rho}|P_{injk} - P_{cylk}|\right)^{1/2}\right) \quad (16)$$

3.4 Injection timing subsystem

The Electronic Control Unit (ECU) activates each fuel injector 4 times per cycle.The fresh charge is internally prepared by injecting fuel twice, the first just before and the second just after the Top Dead Center at the beginning of the suction stroke. This early injection using the same high-pressure CR injection system allows for fuel heating and distribution and gives more time for fuel vaporization and mixing with air. The other two injections are the pilot and main injections that take place before and after the TDC at the start of expansion stroke The following subscripts are used to substitute the subscript i in $\theta_{injection,\ i}$ or $dt_{injection,\ i}$

p is for pilot injection
M is for main injection
1 pre is for first preparation injection
2 pre is for second preparation injection

There are two preparations injections ($\theta_{injection,\ 1\ pre}$ or $dt_{injection,\ 1\ pre}$) and ($\theta_{injection,\ 2\ pre}$ or $dt_{injection,\ 2\ pre}$), pilotinjection ($\theta_{injection,\ p}$ or $dt_{injection,\ p}$) and main injection ($\theta_{injection,\ M}$ or $dt_{injection,\ M}$).

The start and the duration of each injection are obtained by data regression of the experimental data concerning the measurement of the triggering signals of the injector

The pilot injection is just before the Top Dead Centre (TDC) at the end of compression stroke. The small amount of fuel injected triggers the combustion of the fuel already present in the charge. Nearly 2 ms later, the main injection takes place.

The start of pilot injection TS_{p} is calculated from the TDC at the end of compression stroke related to the engine speed and load by the equation

$$TS_p\ [ms] = 0.001017 \times n + 0.00505 \times load - 0.32 \quad (17)$$

The pilot injection duration $dt_{injection,\ p}$ is calculated as a function of engine speed and load from the following equation

$$dt_{injection,\ p}\ [ms] = (5.88\times10^{-5}\times n + 0.003222\times Load + 0.223048)\times (0.00015\times n + 0.002194\times Load + 0.75495) \quad (18)$$

so the end of pilot injection can be determined.

The start of main injection TS_{M} is 2 ms later from the end of pilot injection

The main injection duration $dt_{injection,\ M}$ is calculated as a function of engine speed and load from the following equation

$$dt_{injection,\ M}\ [ms] = ((0.00004\times n + 0.002\times Load + 0.58))\times (0.00015\times n + 0.002194\times Load + 0.75495) \quad (19)$$

Two more short injections are timed just before the end of the exhaust stroke $\theta_{injection,\ 1\ pre}$ and just after the start of the suction stroke $\theta_{injection,\ 2\ pre}$. These to injection control the preparation of the fresh homogenous charge for the next cycle.

The Start of first preparation injection at the end of exhaust stroke of the previous engine cycle TS_{1pre} is adjusted 1.5 ms before the TDC.

$$TS_{\ 1\ pre}\ [ms] = 1.5\ ms \quad (20)$$

The first preparation injection duration $dt_{injection,\ 1pre}$ equal 1 ms at all speeds and loads. So the end of first preparation injection can be determined as 0.5 before TDC.

The start of 2nd preparation injection $TS_{2\ pre}$ is 1 ms later from the end of first preparation injection i. e 0.5 after TDC at the start of suction stroke. The second preparation injection duration $dt_{injection,\ 2pre\ equal}$ 1 ms at all speeds and loads.

The trigger signals before and after the TDC before the suction stroke, (1st and 2nd prepration injections) consist of multiples of very short successive triggers. To account for this disconiuity of the triggered signal a correction coefficient for the area of the injection nozzles during 1st and 2nd prepration injections is established as function of engine speed and load as

$$ACorr. = -0.0000495 \times n + 0.001457 \times Load + 0.19624 \quad (21)$$

All time durations or starting times for injection can be converted to crank angle domain

$$\theta S_{\ i}\ [degree] = 6 \times n \times T_{S\ i}\ [ms] \quad (22)$$

$$\theta_{injection,\ i}\ [degree] = 6 \times n \times dt_{injection,\ i}\ [ms] \quad (23)$$

In the above equations engine speed is in rpm and engine load is in [N.m]

4. Results and Discussions

4.1 Validation for the simulation Results

The model has been conducted using the MATLAB/Simulink environment. The fourth-order Runge-Kutta integration method is adopted. The model parameters shown in table 3have been chosen according to the geometric specifications of the mechanical parts and experimental tests. The available experimental data, dimension of radial piston pump (bore-stroke), dimension of common rail, nozzle diameter of injector, number of the nozzle and speed of the engine, to evaluate the model validity, simulation outputs have been compared with experimental data obtained from a common rail injection diesel engine test rig described above. The available experimental data are the amount of fuel injected per cycle and the fuel line pressure at different engine loads.

Table 3. Model Input Parameters.

	Symbol	**Value**
Fuel density	ρ	870 kg/m^3
High pressure pump plunger diameter	d_p	0.65 cm
High pressure pump plunger stroke	Sp	0.7 cm
The geometric volume of High-Pressure Pump	V_g	0.696 cm^3
The volume of common rail	V_{cr}	20 cm^3
the volume of a single injector	V_{inik}	1.47 cm^3
Area of High-pressure Pump outlet port	Ap_{cr}	0.0707 cm^2
Area of the inlet port of a single injector.	A_{inik}	0.049 cm^2
Injector nozzle orifice diameter	d_n	0.015 cm
The total area of the injector nozzle orifices	A_{iniok}	0.000884 cm^2
The bulk modulus of fuel	E	3.25 Gpa
Discharge coefficients	C_{dcr}, C_{dinik}andC_{diniok}	0.64

Figure 3 shows a comparison between the measured and predicted common rail pressure at different speeds and loads. It is clear that the numerical simulation only predicted the average value of the fuel line pressure with relative error less than 8 % as shown in figure 4 which demonstrates the

relative error between the predicted, and the average value of the measured fuel line pressure and for different speeds and loads.

A comparison between the predicted and measured amounts of fuel injection during one cycle per one cylinder at different engine speeds and loads (30 points) is shown in figure 5. Figure6 shows the relative error of the predicted value compared to the measured value. It is shown that an acceptable agreement between the predicted and experimental results is obtained at all speeds and loads other than 0 and 50 N.m with relative error less than 9 %. The maximum relative error at load of 50 N.m is 13 % while a relative error of 21 % is obtained at 0 N.m load. The relatively large relative error at small loads (0 and 50 N.m) can be attributed to that the model does not simulate the common rail pressure wave fluctuations which affect the quantity of injected fuel. This deficiency combining with the small amount of fuel injected at small loads make the error is higher.

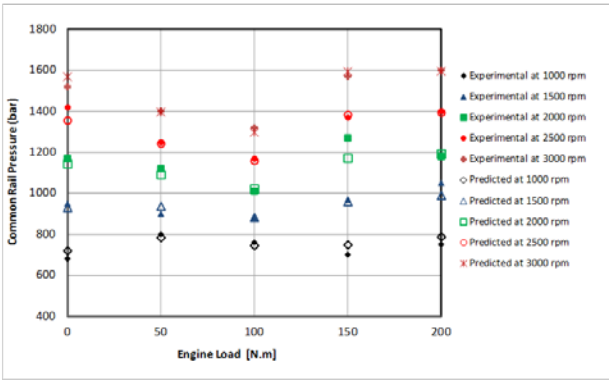

Figure 3. Experimental and predicted common rail fuel pressure at differentspeeds and loads.

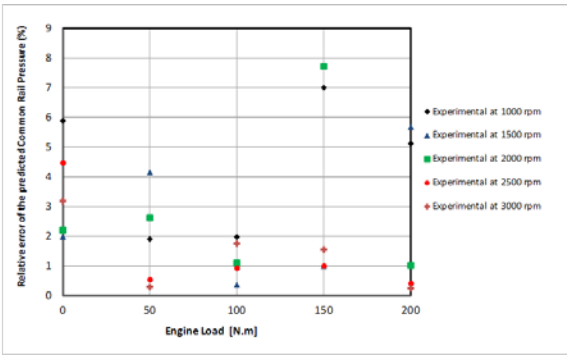

Figure 4. Relative error between the predicted and the average value of the measured fuel line pressure and for different speeds and load.

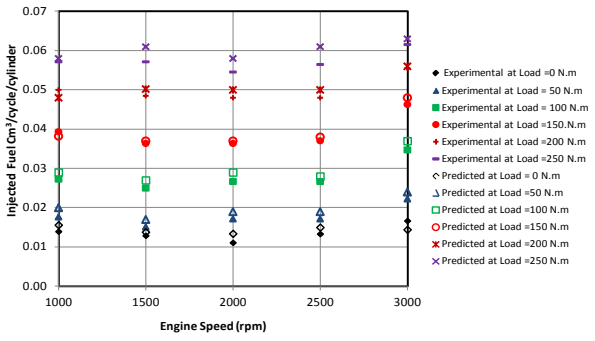

Figure 5. Experimental and predicted injected fuel at different engine speeds and different loads.

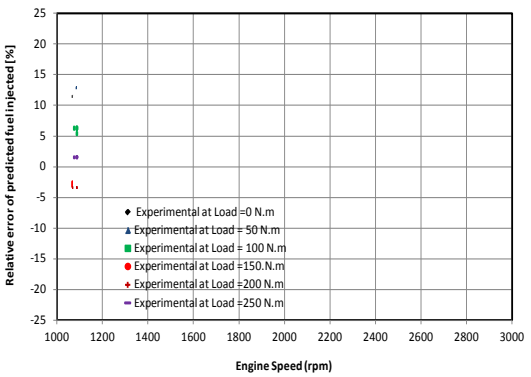

Figure 6. Relative error between the predicted and experimental injected fuel at different enginespeeds and loads.

4.2. Simulation Results

Some simulation results are demonstrated which highlight the modeling capability. Plunger displacement h_p is presented at 3000 rpm in figure 7. The used pump is basically a three-plunger pump derived by the engine crankshaft. The flow rate of the pump exit is regulated by the delivery valve between the high-pressure pump and common rail. As seen in the figure the alternative motion of each piston with the phase shift of 120° between each of them is presented and with the displacement of each piston, the flow rate varies, so from figure 8, the High Pressure Pump outlet flow rate is demonstrated

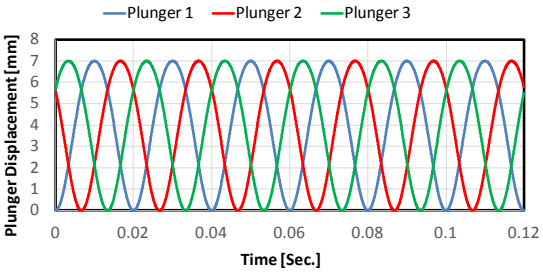

Figure 7. The displacementof the piston plunger.

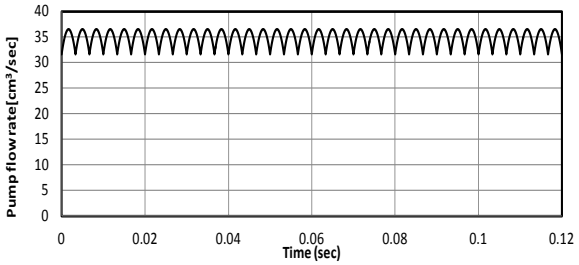

Figure 8. The volumetric high pressure pump flow rate.

Another simulation output is the common rail pressure at different engine speeds and loads. Figure. 9 illustrates the pressure of common rail predicted by Matlab/Simulink at an engine speed of 1500 rpm and load of 250 N.m for three successive cycles as an example. Common Rail pressure is almost constant at about an average value of 1022 bar with a standard deviation of 2.1 bars through the three cycle. Rail pressure fluctuations result from the variations of the fuel supplied from a high-pressure pump, and the quantity of the fuel output to the injectors. These small oscillations shown in figure 10 Occurs at time of injections for the four cylinders. The small oscillations may be attributed to the large Rail volume of 20 cm^3 which is sufficient to provide the desired injection quantity with small pressure variations. Also, the study of the dynamics of common rail pressure wave is not included in this simulation. Payri et al [24], concluded that A lumped model cannot model the rail real dynamics because of the inhomogeneous pressure alternations across the rail length due to the instabilities caused by the incoming flow from the high-pressure pump to rail and the out coming flow to the injectors. This event is mainly intermittent concerning the engine crank angle-scale due to the engine reciprocating motion [25-26]. On the other hand, the pulsation period will vary in the time-scale, if the engine speed varies with time and hence appropriate control of common rail pressure is complicated to realize [27-28].

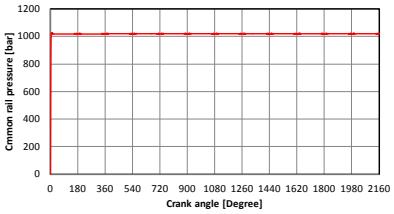

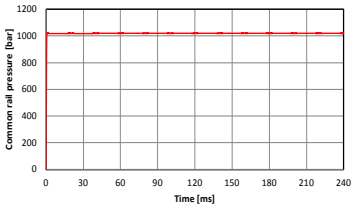

A B

Figure 9. The predicted common rail pressure for three successive cycles (A) in crank angle scale and (B) time scale

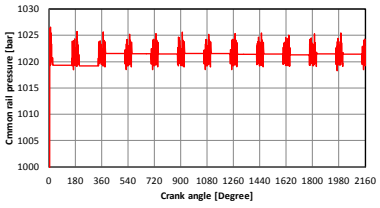

Figure 10. The predicted common rail pressure oscillation in crank angle scale

Figure 11 shows the injection pressure of cylinder no. 2 at engine speed of 1500 rpm and 250 N.m predicted by Matlab/Simulink. The high pressure from the rail-to-injectors pipes right up to the injector entry keeps equal or below the common rail pressure with the existing system layout (both pipes lengths and diameters) so the pressure remains below the durability border of the components. It is noticed that the basic pressure pulsation period (pressure falls due to the injection) is constant on the time-scale due to the constant speed of 1500 rpm on which the engine run so it will be invariant also concerning the engine rotational angle. It is expected to change if the engine speed is changed and this issue will be discussed later.

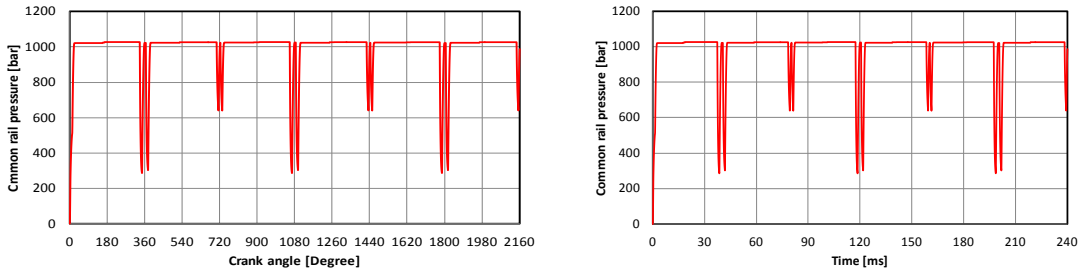

A B

Figure 11. The predicted injection pressure for three successive cycles (A) in crank angle scale and (B) time scale

Figure 12 demonstrates the injected mass flow rate in both the time-scale and crank angle-scale for cylinder no. 2 at engine speed of 1500 rpm and 250 N.m predicted by Matlab/Simulink. The fuel injector solenoid receives a control signal from the Electronic Control Units which stimulates the injector to introduce the fuel into the engine combustion chamber, results in the pressure in the injector to drop. The injection event is principally intermittent on the time-scale and the rotational angle-scale at constant engine speed irrespective of its value. The variation in the duration of the injection in the time scale due to the change in engine speed and load affects the magnitude of the decrease in the common rail and injection pressure [29-30]. This issue will be discussed later. In the rest of this chapter the results will be discussed over one engine cycle other than the first cycle to avoid the effect of transient pressure rise from zero time due to the set initial conditions. This issue will be studied in future work. The predicted injected flow rate profile for one engine cycle is shown in figure 13.

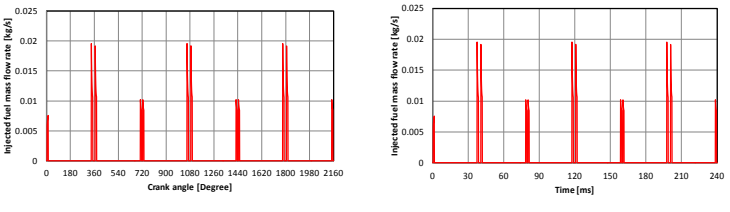

A B

Figure 12. The predicted injected fuel flow rate for three successive cycles (A) in crank angle scale and (B) time scale

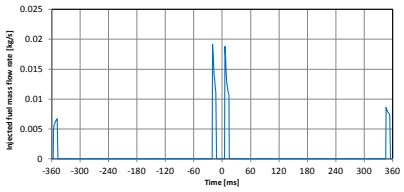

Figure 13. The predicted injected fuel flow rate profile for single cycle cycles in crank angle scale

5. Conclusions

This paper sets out a HPCRS mathematical model for diesel engines. Model equations are generated by using the physical laws governing the fluid-dynamic and mechanical phenomena. The model parameters have been chosen based on the mechanical parts geometric specifications and experimental tests at different operating conditions. The measured in-cylinder pressure obtained from the test rig is used inside the model instead of using a constant value in-cylinder pressure as found in the literature. The injection start time and injection duration are expressed as a function of engine load and speed such that it simulates the change in injection start and duration with engine load and speed.

The proposed model is validated by comparing simulation results with experimental results carried out on diesel engine test rig. The comparison demonstrates the capability of the model to accurately predict the injection system behavior in different operating conditions, in terms of injected flows, and injection pressure.

6. References

[1] Kazutoshi M 1997 *SAE* **970753** 19-29.
[2] Pischinger F 1998 *J. Eng. Gas Turb. Power ASME* **120** pp 641-647.
[3] TennisonP J and Reitz R 2001 *J. Eng. Gas Turb. Power ASME* **123** pp 167-174.
[4] Wang H, Zheng Dand Tian Y 2016 *ISA Transactions* **63** pp 265-273.
[5] Allocca L, Belardini P, BertoliC and Corcione F 1992 *SAE* **920576**.
[6] De Nicolao G, Rossi C, Scattolini R and Suffritti M 1999 *Control Engineering Practice* **7** pp 1061-1069
[7] Maione B, Lino P and Rizzo A 2004 *WSEAS Transactions on Systems* Issue 5, **3** pp. 2164-2169.
[8] Tanner F and Srinivasan S 2009 *Applied Mathematical Modeling* **33** pp 1366–1385
[9] GuoC et al 2018 *Energy Conversion and Management* **160** pp 302–12.
[10] Petranović Z, Sjerić M, Taritaš I, Vujanović M and Kozarac D 2018 *Energy Conversion and Management* **171** pp 1–11.
[11] Zhao F, Yang W, Zhou D, Yu W, Li J and Tay K L 2017 *Fuel* **188** pp 382–9.
[12] Jurića F, Petranovićb Z, Vujanovića M, Katrašnikc T, Viharc R, Wangd X and Neven Duić N 2019 *Energy Conversion and Management* **185** pp 730–739
[13] Chiavola O and Giulianelli P 2001 *SAE Technical Paper* **2001-01-3183**.
[14] Mulemane A, Han J, Lu P,Yoon S and Lai M 2004 *SAE Technical Paper* **2004-01-0536**.
[15] Lino P, Maione B and Rizzo A 2007 *Applied Mathematical Modeling* **31** pp 1770–1784.
[16] IMAGINE SA 2000 *IMAGINE Technical Bulletin* 110, Roanne, France.
[17] Catania A, Dongiovanni C and Mittica A 1992 *J. Eng. Gas Turb. Power ASME* **114** pp 534-543.
[18] Catania A, Dongiovanni C and Mittica A, Negri C and Spessa E 1996, *SAE* **962020**.
[19] Catania A, Dongiovanni C and Mittica A, Negri C and Spessa E 1999, *J. Eng. Gas Turb. Power ASME* **121** pp 186-196.
[20] Lino P, Maione B, and Rizzo A 2005 *IEEE Conference on Emerging Technologies and Factory Automation.*
[21] Dinoi A 2002 Control Problems in Common Rail Diesel Injection Systems (in Italian), Master Theses, Bari.
[22] Kouremenos A, Rakopoulos C, Hountalas D and Kotsiopoulos P 1991 *Proc. ASME-WA Meeting, Atlanta, Georgi*a AES pp. 91-102.
[23] Nikolic B, Kegl B, Markovic S and Melanija S 2012 *Thermal Science* **16** Suppl. 2, pp. S569-S579
[24] Payri F, Lujan J M, Guardiola G and Rizzoni G 2006 *Proc. IMechE-Part D: J Automob. Eng.* **220** pp 347–357.
[25] Chin Y and Coats F1986 *SAE* **860412**.
[26] Yurkovich S and Simpson M 1997 *Proc. Am. Control Conf* pp 278–283.
[27] Sun Z , Zhang Z and Tsao T 2009 *Control Lett.* **58 (6)** pp 452–460.
[28] Zhang Z and Sun Z 2010 *ASME J. Dynam. Syst. Measure. Control* **132 (011004)** pp 1–10.
[29] Coppo M Dongiovanni C and Negri C 2004 *J. Eng. Gas Turb. Power ASME* **126** pp 874–885.
[30] Ubertini S 2006 *J. Eng. Gas Turb. Power ASME* **128** pp 694–701.